

Cytoplasmic localization of prostate-specific membrane antigen inhibitors may confer advantages for targeted cancer therapies.

Matthias, J.; Engelhardt, J.; Schäfer, M.; Bauder-Wüst, U.; Meyer, P.; Haberkorn, U.; Eder, M.; Kopka, K.; Hell, S.; Eder, A.;

Originally published:

April 2021

Cancer Research 81(2021)8, 2234-2245

DOI: <https://doi.org/10.1158/0008-5472.CAN-20-1624>

Perma-Link to Publication Repository of HZDR:

<https://www.hzdr.de/publications/Publ-32347>

Release of the secondary publication
on the basis of the German Copyright Law § 38 Section 4.

Cytoplasmic localization of prostate-specific membrane antigen inhibitors may confer advantages for targeted cancer therapies

Jessica Matthias^{1,2}, Johann Engelhardt¹, Martin Schäfer³, Ulrike Bauder-Wüst³, Philipp T. Meyer^{4,5}, Uwe Haberkorn^{6,7}, Matthias Eder^{4,5}, Klaus Kopka^{3,8,#}, Stefan W. Hell^{1,9}, Ann-Christin Eder^{2,3,4,5*}

¹ Department of Optical Nanoscopy, Max Planck Institute for Medical Research, Heidelberg, Germany

² Helmholtz International Graduate School, German Cancer Research Center, Heidelberg, Germany

³ Division of Radiopharmaceutical Chemistry, German Cancer Research Center, Heidelberg, Germany

⁴ Department of Nuclear Medicine, University Medical Center Freiburg, Faculty of Medicine, University of Freiburg, Freiburg, Germany

⁵ Division of Radiopharmaceutical Development, German Cancer Consortium, partner site Freiburg, Freiburg, Germany and German Cancer Research Center, Heidelberg, Germany

⁶ Department of Nuclear Medicine, Heidelberg University Hospital, Heidelberg, Germany

⁷ Clinical Cooperation Unit Nuclear Medicine, German Cancer Research Center, Heidelberg, Germany

⁸ German Cancer Consortium, Heidelberg, Germany

⁹ Department of NanoBiophotonics, Max Planck Institute for Biophysical Chemistry, Göttingen, Germany

current address: Institute of Radiopharmaceutical Cancer Research, Helmholtz-Zentrum Dresden-Rossendorf (HZDR), Dresden, Germany

Running title

Cytoplasmic localization of PSMA inhibitors

Keywords

Prostate Cancer, Prostate-Specific Membrane Antigen, Dual-Labeled PSMA Inhibitors, Stimulated Emission Depletion Nanoscopy, Theranostics

36 **Financial support**

37 ACE and JM received funding from Helmholtz International Graduate School for
38 Cancer Research PhD stipends. ME and KK received support by the VIP+ grant
39 VP00130, Federal Ministry of Education & Research (BMBF), Germany.

40

41

42 ***Corresponding author**

43 Dr. Ann-Christin Eder

44 University Medical Center Freiburg, Department of Nuclear Medicine

45 Hugstetter Str. 55

46 79106 Freiburg im Breisgau

47 Tel: +49 761 270 63370

48 Fax: +49 761 270 39300

49 Email: ann-christin.eder@uniklinik-freiburg.de

50

51

52 **Conflict of interest**

53 MS, UBW, UH, ME, KK, ACE hold patent rights on dual-labeled PSMA inhibitors. The
54 other authors declare no potential conflicts of interest.

55

56

57 **Additional information**

58 Word count abstract: 188

59 Word count main text: 4963

60 Number of figures: 5

61 Number of tables: 0

62 **Abstract**

63 Targeted imaging and therapy approaches based on novel prostate-specific
64 membrane antigen (PSMA) inhibitors have fundamentally changed the treatment
65 regimen of prostate cancer. However, the exact mechanism of PSMA inhibitor
66 internalization has not yet been studied and the inhibitors' subcellular fate remained
67 elusive. Here, we have investigated the intracellular distribution of peptidomimetic
68 PSMA inhibitors and of PSMA itself by stimulated emission depletion (STED)
69 nanoscopy applying a novel non-standard live cell staining protocol. Our findings
70 confirm PSMA cluster formation at the cell surface of prostate cancer cells and
71 clathrin-dependent endocytosis of PSMA inhibitors. Following the endosomal
72 pathway, PSMA inhibitors accumulate in prostate cancer cells at clinically relevant
73 time points. Strikingly, in contrast to PSMA itself, PSMA inhibitors were found to
74 eventually distribute homogeneously in the cytoplasm – a molecular condition that
75 promises benefits for treatment, as cytoplasmic and in particular perinuclear
76 enrichment of the radionuclide carriers may better facilitate the radiation-mediated
77 damage of cancerous cells. This study is the first to reveal the subcellular fate of
78 PSMA/PSMA inhibitor complexes at the nanoscale and expected to inspire the
79 development of new approaches in the field of prostate cancer research, diagnostics
80 and therapeutics.

81

82 **Statement of significance**

83 This study reveals the subcellular fate of PSMA/PSMA inhibitor complexes close to
84 the molecular level with STED fluorescence nanoscopy. The pioneering insights are
85 of great clinical interest and suggest advantageous targeted therapies.

86 **Introduction**

87 Prostate cancer is the most common type of cancer in men in western societies and
88 is one of the leading causes of cancer-related mortality (1,2). Among prostate cancer
89 biomarkers for imaging and therapy, the prostate-specific membrane antigen (PSMA)
90 has proven to be an excellent target structure due to (i) its overexpression in prostate
91 cancer, (ii) its absence or low expression rates in healthy tissue (3,4) and (iii)
92 increasing expression rates with tumor aggressiveness, androgen-independence,
93 metastatic disease, and disease recurrence (4-9). PSMA is a transmembrane
94 glycoprotein (100–120 kDa) with an extensive extracellular domain (amino acids 44–
95 750), which undergoes clathrin-mediated internalization upon ligand binding (3,10). A
96 novel MXXXL motif of N-terminal amino acids is formed by the cytoplasmic tail
97 mediating PSMA internalization (11). In colocalization studies with internalized
98 transferrin, PSMA was detected in the recycling endosomal compartment upon
99 tracking with the monoclonal antibody mAB J591, which targets the extracellular
100 domain of PSMA (11,12).

101 Specific prostate cancer targeting has been successfully achieved by the
102 development of peptidomimetic PSMA inhibitors. Radiolabeling turns these
103 molecules into powerful tools in the diagnosis and therapy of prostate cancer. In
104 diagnostics of all stages, the ⁶⁸Ga-labeled PSMA inhibitor Glu-urea-Lys(Ahx)-HBED-
105 CC ([⁶⁸Ga]Ga-PSMA-11) has become the most widely used PET/CT imaging agent
106 (13-19).

107 Particularly the metastatic, castration-resistant prostate cancer (mCRPCa) represents
108 a major therapeutic challenge as treatment options are still limited. In therapy of
109 mCRPCa, alpha- or beta-emitter radiolabeled PSMA inhibitors (e.g. PSMA-617,

110 PSMA-I&T) have been introduced as a treatment alternative and first studies have
111 revealed a high efficacy with a favorable safety profile (20,21).

112 The recently developed dual-modality PSMA inhibitors feature two reporter entities
113 (radioactive and/or fluorescent) enabling both preoperative imaging and subsequent
114 intraoperative (radio- or fluorescence-) guidance (22,23). This approach guarantees
115 the precise detection and resection of malignant tissue to the best possible extent,
116 directly affecting treatment outcome and patient survival. The new class of dual-
117 labeled peptidomimetic PSMA inhibitors paves the way for promising new strategies
118 in the diagnosis and therapy of prostate cancer and several of these molecules are
119 currently in preparation for clinical translation (22,23).

120 However, the detailed internalization mechanism and the subcellular distribution of
121 PSMA inhibitors are still unknown. In particular, their intracellular fate is of great
122 clinical interest and crucial for obtaining a detailed understanding of the mechanism
123 of action during endoradiotherapy. Stimulated emission depletion (STED) nanoscopy
124 (24,25) provides the spatial resolution to follow PSMA inhibitor trafficking at the
125 nanoscale. Here, we elucidate the internalization mechanism of PSMA inhibitors and
126 determine their subcellular distribution on the molecular level using STED
127 nanoscopy. For visualizing the intracellular distribution patterns of PSMA inhibitors in
128 relation to PSMA, we developed a novel non-standard live cell immunofluorescence
129 (IF) staining protocol. To the best of our knowledge, this study is the first to
130 investigate and reveal the subcellular fate of PSMA/PSMA inhibitor complexes.

131

132 **Material and Methods**

133 ***Synthesis, radiolabeling and determination of fluorescence properties***

134 The STED-compatible dual-labeled PSMA inhibitors Glu-urea-Lys-HBED-CC-PEG₂-
135 STAR RED and Glu-urea-Lys-HBED-CC-PEG₂-STAR 635P (hereinafter referred to
136 as Glu-urea-Lys-HBED-CC-*<dye>* for *<dye>* conjugates) were synthesized according
137 to previous procedures (22). Radioisotope labeling with ⁶⁸Ga and determination of
138 fluorescence properties were conducted according to previously established
139 protocols. Details on synthesis, radiolabeling and fluorescence spectroscopy are
140 provided in Supplementary Methods.

141

142 ***Cell culture***

143 For cultivation of PSMA-positive androgen-sensitive human prostate adenocarcinoma
144 cells (LNCaP, ATCC CRL-1740, RRID:CVCL_1379, high PSMA expression; 22Rv1,
145 ATCC CRL-2505, RRID: CVCL_1045, moderate/heterogeneous PSMA expression)
146 and PSMA-negative androgen non-reliant human prostate adenocarcinoma cells
147 (PC-3, ATCC CRL-1435, RRID:CVCL_0035), RPMI medium was enriched with 10%
148 FCS and 2 mmol/L L-glutamine (all from PAA). Cells were grown at 37°C in
149 humidified air with 5% CO₂ and were harvested using trypsin-
150 ethylenediaminetetraacetic acid (trypsin-EDTA, 0.25% trypsin, 0.02% EDTA, Gibco,
151 Cat#25200056; <20 passages between thawing and experimental use). Cell line
152 authentication and mycoplasma testing is regularly performed. Authentication of the
153 LNCaP and PC-3 cell lines was confirmed on 03/06/2020. The 22Rv1 cell line was
154 directly obtained from ATCC (purchased on 05/29/2020; Lot: 2215512).

155 Cell binding and internalization experiments were performed as previously described
156 (13). Potential cytotoxicity was assessed by analyzing the duration and frequency of
157 cell division via holographic time-lapse imaging with a HoloMonitor® M4 cytometer
158 (PHI AB). Details to cell binding, internalization and cytotoxicity experiments are
159 provided in Supplementary Methods.

160

161 ***Biodistribution, PET imaging and cryosectioning studies***

162 Biodistribution and PET imaging studies in LNCaP- and PC-3-tumor xenograft mice
163 were performed according to established protocols (22). For cryosectioning, tissue
164 was directly frozen 1 h after tracer injection (details in Supplementary Methods). All
165 experiments complied with the current laws of the Federal Republic of Germany and
166 were conducted according to German Animal Welfare guidelines and ARRIVE
167 guidelines. The experiments were approved by the regional authorities
168 *Regierungspräsidium Karlsruhe* and *Freiburg* (approval numbers G158/15, G18/04).

169

170 ***STED and confocal microscopy***

171 All confocal and STED data were acquired with a custom-built STED system close to
172 the one published by Gorlitz et al. (26) (details in Supplementary Methods).

173 For assessing the time and concentration dependence of PSMA inhibitor
174 internalization, cells were incubated with 50/100/250/500 nM Glu-urea-Lys-HBED-
175 CC-STAR RED in RPMI for 5/15/30/45 min at room temperature. To verify specific
176 uptake, cells were co-incubated with 2-PMPA (500 µM). Additionally, potential
177 internalization of free dye was tested by incubating cells with STAR RED and
178 STAR 635P carboxylic acid (Abberior, Cat#STRED-0001, Cat#ST635P-0001) for 1 h

179 at 37°C. After fixation with paraformaldehyde (2% PFA in PBS) for 10 min, the
180 samples were mounted with ProLong Diamond Antifade Mountant containing DAPI
181 (Thermo Fisher Scientific, Cat#P36966).

182 For live cell imaging and colocalization experiments, a novel non-standard live cell
183 staining protocol exploited the blocking effect of low temperatures on PSMA
184 internalization without impairing cell health. Briefly, cells were immunolabeled against
185 PSMA and/or incubated with dual-labeled PSMA inhibitors on ice to specifically target
186 the entire cell membrane-bound PSMA fraction. Internalization of the
187 antibody/PSMA/PSMA inhibitor complex was triggered by temperature increase. For
188 PSMA IF, a monoclonal anti-PSMA antibody (1:50, mouse IgG1, clone 107-1A4,
189 Sigma-Aldrich, Cat#SAB4200257, RRID:AB_11129838) and a STAR 600-labeled
190 goat anti-mouse-IgG antibody (1:50, Abberior, Cat#2-0002-010-5) were used. For
191 colocalization experiments with clathrin, LNCaP cells were transiently transfected
192 with the fusion construct SNAP-tag/clathrin light chain (SNAP-CLC) and stained with
193 the live dye 610CP-BG (27,28). Clathrin-mediated endocytosis was blocked via co-
194 incubation with 30 μ M Pitstop 2 (Sigma-Aldrich, Cat#SML1169). For endosomal
195 colocalization experiments, LysoTrackerTM Green DND-26 (Thermo Fisher Scientific,
196 Cat#L7526) or SiR-lysosome (SPIROCHROME, Cat#SC012) were used. Details on
197 microscopy sample preparation and colocalization experiments are provided in
198 Supplementary Methods.

199 Background correction was done by subtracting at most 10% of the maximum
200 fluorescence signal. Linear deconvolution (Wiener filter) was applied with a
201 Lorentzian PSF (FWHM STED PSF 60 nm, FWHM confocal PSF 200 nm) and only
202 to the extent that data are smoothed and noise is reduced but resolution is not

203 increased. Detailed information on microscopy data analysis are provided in
204 Supplementary Methods.

205 ***Flow cytometry studies on PSMA binding affinity and pH dependence***

206 The binding affinity of Glu-urea-Lys-HBED-CC-STAR RED and -STAR 635P
207 (0.0/0.5/1.0/2.5/5.0/10/25/50/100/500 nM) to PSMA on LNCaP and 22Rv1 cells was
208 determined as the mean effective concentration (EC₅₀) by flow cytometry (BD FACS
209 Canto II Flow Cytometer, BD Biosciences). To demonstrate the specificity of the
210 binding, all conjugates in concentrations of 0.5/5.0/50 nM were additionally co-
211 incubated with 500 μM 2-PMPA. The pH dependence of the binding was analyzed for
212 Glu-urea-Lys-HBED-CC-STAR RED, -STAR 635P and the antibody complex
213 (primary antibody: monoclonal anti-PSMA, mouse IgG1, clone 107-1A4, Sigma-
214 Aldrich, Cat#SAB4200257, RRID:AB_11129838; secondary antibodies: STAR 600-
215 or STAR RED-labeled goat anti-mouse-IgG, Abberior, Cat#2-0002-010-5 or Cat#2-
216 0002-011-2, RRID:AB_2810982). Details on the flow cytometry studies are provided
217 in Supplementary Methods.

218

219 ***Statistical aspects and data presentation***

220 Experiments were performed at least in triplicate. Quantitative data in text are
221 expressed as mean ± standard deviation (SD). Bar plots depict the mean ± SD of the
222 measurements for replicate experiments. Box plots indicate the interquartile range
223 (box), the outer-most data points falling within 1.5× interquartile range (whiskers), the
224 median (center line) and the mean (triangle) of the measurements for replicate
225 experiments. If applicable, means were compared using Student's t test (GraphPad
226 Prism Version 7, GraphPad Software, Inc.). P-values < 0.05 were considered
227 statistically significant.

229 **Results**

230 ***STED-Compatible Dual-Labeled PSMA Inhibitors Feature High PSMA Affinity***
231 ***and Specific Internalization Properties In Vitro.***

232 STED-compatible dual-labeled PSMA inhibitors were derived from Glu-urea-Lys-
233 HBED-CC-PEG₂-IRDye800CW, as the latter preclinically performs comparably to
234 clinically established molecules (e.g. PSMA-11 or PSMA-617) (13,22,29,30). The
235 analytical data of the final products Glu-urea-Lys-HBED-CC-PEG₂-STAR RED and
236 Glu-urea-Lys-HBED-CC-PEG₂-STAR 635P are summarized Table S1, their
237 structures are shown in Fig. 1A, and their fluorescence spectra are displayed in Fig.
238 S1.

239 Incubation of LNCaP (high PSMA expression) and 22Rv1 (moderate/heterogeneous
240 PSMA expression) cells with ⁶⁸Ga-labeled Glu-urea-Lys-HBED-CC-STAR RED and -
241 STAR 635P resulted in significant and specific binding to PSMA with affinities in the
242 low nanomolar range. Additionally, both conjugates specifically internalized (Table
243 S2). The pronounced difference in PSMA expression levels (31) accounts for the
244 reduced signal of 22Rv1 cells. This trend is likewise reflected in all following
245 fluorescence imaging experiments.

246 To ascertain and elaborate on the radioactively determined *in vitro* data, cell binding
247 and internalization was investigated in confocal microscopy experiments (Fig. 1B). All
248 subsequent fluorescence microscopy data were acquired with Glu-urea-Lys-HBED-
249 CC-STAR RED, as this conjugate displayed superior photostability and contrast in
250 the fluorescence imaging experiments. Confocal imaging detected an increasing
251 accumulation of Glu-urea-Lys-HBED-CC-STAR RED in PSMA-positive cells
252 independent of its concentration over time (Fig. S2). A blocking effect was not
253 detected for the tested concentration range (50 nM to 500 nM). Blocking studies in

254 the presence of 500 μ M 2-PMPA, internalization experiments with the free Abberior
255 dyes STAR RED and STAR 635P and with PSMA-negative PC-3 cells proved the
256 specificity of PSMA binding and internalization (Fig. S3A-D).

257 For confocal time-lapse experiments, LNCaP cells were incubated with Glu-urea-Lys-
258 HBED-CC-STAR RED for 20 min on ice to prevent premature internalization,
259 subsequently washed and immediately imaged. Over a period of 120 min, steady
260 internalization was observed (Fig. S3E and F, Movie S1). No morphological changes
261 or other signs of impaired cell viability were detected during the experiment. To
262 rigorously exclude cytotoxicity by the PSMA inhibitor, the frequency and duration of
263 cell division was assessed via holographic time-lapse imaging. Cell proliferation was
264 followed in the presence of either Glu-urea-Lys-HBED-CC-STAR RED or -
265 STAR 635P for 48 h and was compared to the proliferation of untreated cells. The
266 data show no evidence of cytotoxicity but a slightly accelerated LNCaP cell
267 proliferation in the presence of PSMA inhibitors (Fig. 1C and D, Fig. S4, Fig. S5,
268 Table S3, Movie S2-S4).

269

270 ***LNCaP Xenograft Tumors in Mice are Specifically Targeted by STED-***
271 ***Compatible Dual-Labeled PSMA Inhibitors.***

272 The ability of Glu-urea-Lys-HBED-CC-STAR RED and -STAR 635P to specifically
273 target PSMA *in vivo* was evaluated in biodistribution studies at 1 h post injection
274 (p.i.). Both conjugates performed similarly in a PSMA-expressing LNCaP tumor
275 mouse xenograft model with a high tumor uptake of around 5 %ID/g and a favorable
276 organ distribution profile comparable to PSMA-11, the reference compound without
277 dye (30) (Fig. 2A, Table S4). Confocal imaging of tumor and muscle tissue
278 cryosections confirmed a PSMA-specific uptake and revealed a homogenous

279 subcellular distribution pattern throughout the tumor cells already 1 h p.i. (Fig. 2B).
280 The specificity of the *in vivo* tumor uptake of Glu-urea-Lys-HBED-CC-STAR RED
281 was further proven with PSMA-negative PC-3 tumor xenografts. The uptake in
282 PSMA-negative tumor tissue was comparable to the uptake in muscle tissue (Table
283 S5).

284 Additionally, small-animal PET imaging was performed with ⁶⁸Ga-labeled Glu-urea-
285 Lys-HBED-CC-STAR RED. Selective tumor uptake in the LNCaP xenograft model
286 accompanied by rapid clearance from off-target tissue resulted in a high imaging
287 contrast at early time points. In PSMA-negative PC-3 xenografts, no measurable
288 uptake of the conjugate was observed during the experiment, demonstrating high
289 PSMA specificity (Fig. 2C). The corresponding time activity curves showed rapid
290 clearance from muscle, liver and heart tissues, but continuous accumulation of the
291 conjugate in kidneys and bladder confirming the renal elimination (Fig. 2D).

292

293 ***Clathrin Mediates the Internalization of PSMA Inhibitors after PSMA Binding.***

294 To resolve details of the PSMA distribution in the cell membrane, Glu-urea-Lys-
295 HBED-CC-STAR RED bound PSMA was imaged with STED nanoscopy. A
296 heterogeneous distribution of the fluorescence signal along the cell membrane was
297 observed, suggesting areas of higher and lower PSMA density, which could not be
298 visualized with confocal imaging. Within the patches of high PSMA density, round to
299 oval-shaped PSMA clusters of various sizes were detected (Fig. 3A, Fig. S6A).

300 After short internalization times, the PSMA inhibitor signal was localized to the
301 membrane of cytoplasmic vesicles. While confocal imaging visualized the vesicles as
302 blurred diffraction-limited spots, STED imaging enabled the nanometer resolution of

303 defined, hollow, spherical structures (Fig. 3B and C). Heterogeneous vesicle
304 distribution was observed with regions of higher and lower vesicle density. While the
305 nucleus always remained free of any Glu-urea-Lys-HBED-CC-STAR RED signal, the
306 overall concentration of vesicles in cellular filopodia increased particularly (Fig. 3D).
307 Line profiles of vesicles derived from raw confocal and STED data confirm the
308 improvement in resolution gained by STED. The full width half maxima (FWHMs) of
309 the Lorentzian fits suggest a spatial resolution significantly below the diffraction limit
310 (Fig. 3C, Fig. S6B and C; for postprocessing of STED data refer to Fig. S7).

311 Live LNCaP cell confocal colocalization experiments between Glu-urea-Lys-HBED-
312 CC-STAR RED and SNAP-tagged CLC labeled with 610CP (27,28) showed a
313 significant signal overlap for early time points that decreased with progressing
314 internalization time (Fig. 3E, Fig. S8A). The Pearson's correlation coefficient (PCC)
315 (32) dropped significantly within the first 15 min of internalization, suggesting clathrin-
316 mediated uptake with rapid clathrin uncoating after internalization (Fig. 3F, Table S6),
317 which enabled the fusion with early endosomes and thus vesicle growth (33,34). Co-
318 incubation with the clathrin inhibitor Pitstop 2 confirmed clathrin-dependent PSMA
319 inhibitor internalization (Fig. S8B and C).

320 As clathrin coated vesicles (CCVs) feature a well-defined diameter, the diameter of
321 endocytic vesicles is an indicator for the degree of progress along the endocytic
322 pathway. It was analyzed by fitting a two-dimensional ring function to the
323 fluorescence signal (Fig. S6D). The average diameter does not differ significantly
324 within the first hour of internalization. The large SDs indicate a broad spread of
325 diameter in the overall vesicle population, especially for later times (Fig. 3G, Table
326 S7). These values are in the range of but, especially for LNCaP cells, always larger
327 than the size of CCVs as published in the literature (35,36).

328

329

330 ***PSMA Inhibitors Distribute Homogeneously in the Cytoplasm Over Time.***

331 For assessing the extent and duration of colocalization of the PSMA inhibitors with
332 PSMA during and after the internalization process, incubation with Glu-urea-Lys-
333 HBED-CC-STAR RED was combined with indirect immunolabeling of PSMA with the
334 Abberior dye STAR 600 in a novel non-standard live cell staining protocol. To avoid
335 premature PSMA internalization, living cells were stained on ice and internalization
336 times were well defined by subsequent incubation at 37°C (Fig. 4A, Fig. S9). The
337 PSMA inhibitor and the primary/secondary antibody complex were both internalized
338 without any evidence for mutual blocking effects. The intracellular distribution of the
339 PSMA inhibitor and PSMA was visualized for different internalization times by STED
340 (LNCaP) and confocal (22Rv1) microscopy.

341 Due to biological heterogeneity, we rather state qualitative trends than quantitative
342 numbers. Colocalization trends can be illustrated in pixel fluorograms (37)
343 (hereinafter referred to as fluorograms; for details, see Supplementary Methods). For
344 visualizing the time-dependent changes in the colocalization of PSMA inhibitor and
345 PSMA, we subdivided the fluorograms of all dual color STED/confocal images in
346 three defined sections separating (i) the PSMA antibody signal only (top section), (ii)
347 the colocalizing signal (middle section) and (iii) the PSMA inhibitor signal only
348 (bottom section). The background (quarter circle in bottom left corner) was set to the
349 average intensity of Glu-urea-Lys-HBED-CC-STAR RED after 24 h of internalization
350 (Fig. 4B).

351 For short internalization times, the PSMA inhibitor signal (red) and the PSMA
352 antibody signal (cyan) strongly colocalized in one fraction (white) falling into the
353 middle section of the fluorogram representing specific binding of the PSMA inhibitor
354 to PSMA in the plasma and vesicle membrane (Fig. 4C, Fig. S10). The
355 corresponding PCC peaked at 30 min with $r(\text{LNCaP})=0.65\pm 0.08$ ($N=9$) and
356 $r(22\text{Rv}1)=0.70\pm 0.06$ ($N=15$). During the first hour of internalization, continuing
357 colocalization of the signals at the membrane of cytoplasmic vesicles was detected
358 with an average PCC of $r(\text{LNCaP})=0.54\pm 0.09$ ($N=43$) and $r(22\text{Rv}1)=0.65\pm 0.07$
359 ($N=56$).

360 However, around 45 min, the cyan fraction (PSMA antibody) started to increase
361 significantly in the fluorogram's top section and the red fraction (PSMA inhibitor)
362 started to slowly vanish into the background. Over time, the relative intensities of both
363 signals in the foreground of the middle section of the fluorogram, and thus the
364 colocalizing fraction, significantly declined. The relative intensity of the PSMA
365 inhibitor in the entire foreground of the fluorogram (all three sections taken together)
366 significantly decreased while it increased in the entire background. However, the
367 relative intensity of PSMA changed neither in the entire foreground nor in the entire
368 background (Fig. 4C, Fig. S10, Fig. S11A-E).

369 These trends illustrate the gradual release of the PSMA inhibitor from PSMA. The
370 PSMA inhibitor signal initially distributed homogeneously in the vesicles (Fig. 4D) and
371 finally dispersed in the cytoplasm after >3 h of internalization (Fig. 4E and F, Fig.
372 S11F, Table S8). At these times, the PSMA antibody signal was still detected at the
373 vesicle membrane and additionally in dotted patches at the cell membrane,
374 presumably representing recycled PSMA (see next subsection).

375 At later time points (6 h, 24 h), no significant further changes of the signal distribution
376 were observed (Fig. S11A-F) and the colocalization between PSMA inhibitor and
377 PSMA was significantly reduced with an average PCC of $r(\text{LNCaP})=0.25\pm 0.12$
378 ($N=18$) and $r(22\text{Rv}1)=29\pm 0.15$ ($N=21$). Photobleaching was found to be negligible as
379 the ratio of the integrated fluorescence intensities did not drastically change over time
380 with an average of 1.17 ± 0.35 (LNCaP $N=57$, PSMA to PSMA inhibitor). Dye-
381 dependent effects could be excluded by substantiating the results of Glu-urea-Lys-
382 HBED-CC-STAR RED with Glu-urea-Lys-HBED-CC-STAR 635P and the results of
383 PSMA STAR 600 IF with PSMA STAR RED IF (Fig. S11G and H).

384

385 ***PSMA Is Recycled in the Endosomal Compartment.***

386 To obtain more information on the PSMA recycling pathway, endosomal
387 colocalization experiments were carried out. Living cells were immunolabeled for cell
388 membrane-bound PSMA on ice to prevent premature PSMA internalization.
389 Subsequently, internalization was triggered by incubation at 37°C. After different
390 internalization times, endosomal colocalization was assessed during live cell confocal
391 imaging experiments by staining with LysoTracker™ Green DND-26, which is
392 selective for both lysosomes and endosomes. With progressing internalization time,
393 the PSMA signal increasingly overlapped with the endosomal signal and the
394 respective PCC significantly climbed (Fig. 5A and B, Table S9), suggesting
395 endosomal recycling of PSMA. Non-colocalizing LysoTracker signal was additionally
396 detected due to unlabeled PSMA and non-PSMA-carrying lysosomes (Movie S5).
397 Co-incubation with 2-PMPA, Glu-urea-Lys-HBED-CC-STAR RED or -STAR 635P did
398 not significantly affect the degree of colocalization (Table S9). PSMA recycling was
399 further supported by the occurrence of clustered PSMA antibody signals at the cell

400 membrane not colocalizing with PSMA inhibitor in confocal and STED imaging
401 experiments after 45 min of internalization (Fig. 5C).

402 The results were confirmed in live confocal and live STED colocalization experiments
403 by co-staining with SiR-lysosome, which also targets both lysosomes and
404 endosomes (Fig. S12A, Movie S5). To exclude phototoxic influence, low light
405 intensity confocal times-series of lysosomal dynamics were recorded after STED
406 imaging. No qualitative difference in lysosomal movement was observed compared to
407 control cells not exposed to high STED laser intensities (Movie S6 and S7).

408 ***PSMA Binding is pH Dependent.***

409 The homogeneous cytoplasmic distribution of Glu-urea-Lys-HBED-CC-STAR RED
410 for internalization times >3 h suggested a separation of the PSMA/PSMA inhibitor
411 complex in the endosomes by decreasing pH. To test this hypothesis, the pH
412 dependence of the binding properties of the PSMA antibody and the PSMA inhibitor
413 to PSMA on LNCaP cells were assessed. In flow cytometry studies, the fractions
414 bound at different physiologically relevant pH values in percent of the fraction bound
415 at pH 7.0 were measured via the detected fluorescence signal of the PSMA inhibitors
416 or the secondary antibodies. The binding of the antibody complexes (primary
417 monoclonal anti-PSMA antibody decorated with secondary antibody conjugated to
418 Abberior STAR 600 or Abberior STAR RED) to PSMA was not significantly affected
419 up to an acidic pH of 4.6. In contrast, the binding of Glu-urea-Lys-HBED-CC-
420 STAR RED and -STAR 635P to PSMA was drastically reduced with increasing acidity
421 (Fig. 5D, Tables S10 and S11). Temperature and/or pH dependent fluorophore
422 degradation of the PSMA inhibitors could be excluded (Fig. S12B and C).

423

424 **Discussion**

425 PSMA-targeted imaging and therapy has refashioned the diagnosis and the
426 treatment of prostate cancer patients over the last years (14-16,19). In particular,
427 endoradiotherapy with alpha- or beta-emitter radiolabeled PSMA inhibitors offers a
428 promising treatment approach for late stage mCRPCa patients beyond established
429 treatment options (20,21).

430 With the development of dual-labeled PSMA inhibitors, an additional imaging
431 modality has been successfully introduced to the clinical routine (22,23,38). Besides
432 intraoperative fluorescence-guided surgery, the additional fluorescence property
433 enables intracellular tracking of the dual-labeled inhibitor, making it a perfect model
434 compound for analyzing the subcellular fate of peptidomimetic PSMA inhibitors at the
435 nanoscale. To the best of our knowledge, the detailed subcellular fate of PSMA/
436 PSMA inhibitor complexes for peptidomimetic PSMA inhibitors has not been
437 investigated with fluorescence nanoscopy so far.

438 All existing knowledge on the mechanism of internalization and the intracellular
439 distribution of PSMA is solely based on diffraction-limited confocal microscopy
440 studies (11,12). The herein achieved spatial resolution is indeed sufficient to follow
441 the coarse localization of PSMA and its inhibitors inside cells over time. However, to
442 precisely investigate localization subtleties (e.g. cluster substructures) and to
443 elucidate in detail the subcellular fate of PSMA and PSMA inhibitor (e.g. molecular
444 colocalization), STED nanoscopy is the method of choice, as it combines the required
445 spatial resolution with inherently coaligned fluorescence imaging channels (excitation
446 multiplexed, one STED donut) (39).

447 Since this nanoscopy technique places special demands on the fluorophores used
448 (40), we synthesized dual-labeled PSMA inhibitors based on PSMA-11 equipped with
449 the STED-compatible Abberior dyes STAR RED and STAR 635P. Both conjugates
450 exhibited high PSMA-specific binding affinities, specifically internalized fractions,
451 specific tumor uptake in PSMA-positive lesions and high tumor-to-background ratios
452 at early time points comparable to the parental structure (22) and reference
453 compounds without dye (13,29). Hence, the additional fluorescence moiety does not
454 affect the main characteristics of our conjugates (e.g. pharmacokinetic properties,
455 tumor accumulation), making them suitable for mimicking clinically used PSMA
456 inhibitors to study their intracellular fate with STED nanoscopy.

457 Confocal and STED imaging as a function of time permitted the visualization of the
458 intracellular distribution of PSMA and of our PSMA inhibitors in PSMA-expressing
459 LNCaP and 22Rv1 cells. The data revealed an increase of the internalized PSMA
460 inhibitor fraction over time, independently of the concentrations tested. These results
461 support the radioactively determined *in vitro* data acquired with the ⁶⁸Ga-labeled
462 PSMA inhibitors in cell binding and internalization studies.

463 Long-term PSMA inhibitor internalization experiments using confocal and STED
464 imaging indicate enrichment in cells. These findings are in line with the *in vivo* time
465 course of tumor accumulation, which agrees with our observations of a long-term
466 accumulation of our PSMA inhibitors in prostate cancer tumor cells with a high signal-
467 to-background ratio. Non-specific signal of unbound inhibitors decreased over time,
468 while the signal of the specifically internalized fraction remained. Targeting of non-
469 tumor tissue was very limited, but even if off-target internalization were to occur, our
470 holographic cytometry data does not indicate cytotoxic effects by the non-
471 radiolabeled PSMA inhibitors.

472 STED nanoscopy allowed the visualization of structural subtleties of the cell
473 membrane-bound PSMA fraction (assessed with both PSMA IF and PSMA inhibitor).
474 The PSMA signal was not homogeneously distributed along the cell membrane, but
475 rather spread into patches of oval- to round-shaped signals of different sizes, both
476 before internalization and after PSMA recycling. We assume that these individual
477 signals consist of varying numbers of PSMA molecules grouped in clusters at the cell
478 membrane. PSMA clustering at the cell surface was previously suggested based on
479 data of biochemical assays, in which it was artificially induced with antibodies. PSMA
480 clustering is crucial not only for PSMA activation and its subsequent internalization,
481 but also for many downstream signalling pathways directly or indirectly affecting cell
482 proliferation (41-43) potentially explaining the slightly accelerated LNCaP division
483 frequency and duration we observed.

484 With STED nanoscopy, we visualized PSMA clustering at the cell surface for the first
485 time, induced either by antibodies or by our PSMA inhibitors. During the LysoTracker
486 colocalization experiments, we did not observe significant differences in endosomal
487 colocalization in the presence or absence of our PSMA inhibitors, as PSMA
488 clustering, activation and internalization was in any case induced by our PSMA IF
489 labeling approach.

490 During the early phase of the internalization process, cytoplasmic vesicle formation
491 was observed. Live cell colocalization experiments suggest that the PSMA-specific
492 internalization of peptidomimetic PSMA inhibitors is mediated via clathrin-dependent
493 endocytosis. As resolved by STED imaging, the average vesicle diameter is more
494 than twice the value for CCVs found in literature (35,36) but the large SD indicates a
495 very heterogeneous vesicle population in our samples. The FWHMs of selected
496 vesicle line profiles suggest a resolution good enough to resolve vesicles with

497 approx. 100 nm in diameter. Thus, we assume that we mostly detected early
498 endosomes, as CCVs quickly uncoat and fuse to become early endosomes with
499 diameters larger than CCVs. We could indeed confirm that PSMA itself passes the
500 endosomal pathway to be either degraded in lysosomes or recycled back to the cell
501 surface as previously described (10,11).

502 Furthermore, we developed a novel non-standard live cell IF staining protocol to
503 visualize the intracellular distribution of our PSMA inhibitors in relation to PSMA. In
504 general, antibody staining is limited to fixed cells as antibodies are not cell membrane
505 permeable. Here, we exploited the fact that PSMA internalization can be blocked by
506 low temperature without impairing cell health. Thus, the entire cell membrane-bound
507 PSMA fraction could be labeled by incubating the cells on ice. A subsequent
508 temperature increase triggered the internalization of the antibody/PSMA/PSMA
509 inhibitor complex (Fig. S9). While indirect IF provides strong signal amplification, our
510 PSMA inhibitors add only one fluorophore per PSMA molecule. Despite this
511 difference in fluorophore stoichiometry, the brightness and signal-to-noise ratio of the
512 PSMA inhibitor signal is only slightly reduced to the immunolabeled PSMA signal.

513 Interestingly, peptidomimetic PSMA inhibitors appear to distribute fundamentally
514 differently on the subcellular level than PSMA antibodies used for prostate cancer
515 immunotherapy. For short internalization times, strong colocalization was observed
516 between PSMA and our PSMA inhibitors, but it decreased over time and eventually
517 vanished at later time points. The PSMA/PSMA inhibitor complex dissociates during
518 the PSMA recycling process in the endosomal compartment allowing the PSMA
519 inhibitors initially to distribute in the endosomes but to disperse gradually
520 homogeneously in the cytoplasm without binding to other structures. Immunolabeled
521 PSMA remained in the vesicle membrane, eventually to be recycled back to the cell

522 membrane. Rajasekaran *et al.* previously reported on internalization and vesicle
523 formation of antibody-targeted PSMA after 2 h of incubation (11). Our findings match
524 these results but additionally visualize PSMA localization at later time points up to
525 24 h.

526 A dye-dependent effect could be excluded by interchanging the fluorescent labels for
527 immunolabeled PSMA and PSMA inhibitor. It could additionally be shown that the
528 spectral properties of our PSMA inhibitors were not sensitive to acidic pH or elevated
529 temperature and, as unnatural inhibitors of PSMA, our conjugates are presumably
530 intrinsically inert to lysosomal digestion.

531 Remarkably, significant differences in the binding affinity to PSMA at acidic pH were
532 detected between the antibody and PSMA inhibitor. The interaction between PSMA
533 and PSMA inhibitor decreased drastically at acidic pH, whereas binding of the anti-
534 PSMA antibody/secondary antibody complex remained unaffected. The difference in
535 pH sensitivity of PSMA binding is one plausible explanation for the fundamentally
536 different intracellular distributions observed for the antibody and PSMA inhibitor. With
537 decreasing endosomal pH, the PSMA binding affinity of the PSMA inhibitors is
538 reduced, shifting the equilibrium between bound and unbound PSMA inhibitor
539 towards the unbound state. We now speculate that, at endosomal pH, the acidic
540 moieties of PSMA inhibitors are mostly protonated, allowing for endosomal escape
541 and cytoplasmic dispersion. Following this hypothesis, unbound PSMA inhibitor
542 would be continuously removed from the PSMA bound/unbound collective inside the
543 endosomes. By pushing the position of the equilibrium further towards the unbound
544 state, eventually, the entire PSMA inhibitor population would be located inside the
545 cytoplasm, a process simply driven by entropy. Finally, the cytoplasm's neutral pH is
546 assumed to trap the PSMA inhibitors inside the cell by deprotonating their acidic

547 moieties, thereby restoring the molecules' membrane impermeability. However,
548 further studies on externalization and membrane permeability need to confirm this
549 hypothesis.

550 The performance of prostate cancer targeting inhibitors in diagnostics and therapy
551 highly depends on their cell binding and internalization properties as well as on their
552 subcellular localization. This study describes the intracellular distribution of PSMA
553 and peptidomimetic PSMA inhibitors at the nanometer scale for the first time. STED
554 fluorescence nanoscopy allows insights into the internalization and precise
555 localization of both PSMA inhibitors and of PSMA itself at clinically relevant time
556 points. As observed in this study, strong and specific internalization in combination
557 with a long retention allows the inhibitors' enrichment in the target cells over time
558 affording high imaging contrasts while sparing healthy tissue and preventing off-
559 target tissue effects. The striking difference between the PSMA antibodies' and the
560 PSMA inhibitors' subcellular fate will potentially have significant impact on the
561 therapeutic efficiency of the peptidomimetic inhibitors. The homogeneous dispersion
562 of PSMA inhibitors in prostate cancer cells after internalization, which we have
563 demonstrated here for the first time, is of particular interest in endoradiotherapy, for
564 which this dispersed cytoplasmic distribution potentially leads to beneficial effects.
565 Intracellular accumulation and localization in nuclear proximity may allow a more
566 target-oriented application of effectively higher local radiation doses – especially with
567 high linear energy transfer alpha particles - resulting in potent DNA damage and
568 subsequent apoptosis.

569 We expect our results to fuel further ligand development, not only in the field of
570 prostate cancer. Our findings will hopefully boost the development of refined and/or

571 new targeting strategies for diagnostic and therapeutic approaches in prostate cancer
572 and other human cancer treatment.

573 **Acknowledgments**

574 We acknowledge funding from Helmholtz International Graduate School for Cancer
575 Research PhD stipends for ACE and JM and support by the VIP+ grant VP00130,
576 Federal Ministry of Education& Research (BMBF), Germany. We thank Karin Leotta,
577 Ursula Schierbaum and Mareike Roscher for support in biodistribution and small-
578 animal imaging studies, Martin Seefeld for providing access to UV/Vis and
579 fluorescence spectrophotometers, Alexey Butkevich and Vladimir Belov for providing
580 the fluorescent live dye 610CP-BG, Francesca Bottanelli for providing the SNAP-CLC
581 construct, Steffen J. Sahl and Jade Cottam Jones for helpful discussions, and Rifka
582 Vlijm for support in data analysis.

583 **References**

- 584 1. Ferlay J, Steliarova-Foucher E, Lortet-Tieulent J, Rosso S, Coebergh JW,
585 Comber H, *et al.* Cancer incidence and mortality patterns in Europe: estimates
586 for 40 countries in 2012. *Eur J Cancer* **2013**;49:1374-403.
- 587 2. Siegel RL, Miller KD, Jemal A. Cancer statistics, 2019. *CA Cancer J Clin*
588 **2019**;69:7-34.
- 589 3. Ghosh A, Heston WD. Tumor target prostate specific membrane antigen
590 (PSMA) and its regulation in prostate cancer. *J Cell Biochem* **2004**;91:528-39.
- 591 4. Silver DA, Pellicer I, Fair WR, Heston WD, Cordon-Cardo C. Prostate-specific
592 membrane antigen expression in normal and malignant human tissues. *Clin*
593 *Cancer Res* **1997**;3:81-5.
- 594 5. Wright GL, Jr., Haley C, Beckett ML, Schellhammer PF. Expression of
595 prostate-specific membrane antigen in normal, benign, and malignant prostate
596 tissues. *Urologic oncology* **1995**;1:18-28.
- 597 6. Sweat SD, Pacelli A, Murphy GP, Bostwick DG. Prostate-specific membrane
598 antigen expression is greatest in prostate adenocarcinoma and lymph node
599 metastases. *Urology* **1998**;52:637-40.
- 600 7. Mhawech-Fauceglia P, Zhang S, Terracciano L, Sauter G, Chadhuri A,
601 Herrmann FR, *et al.* Prostate-specific membrane antigen (PSMA) protein
602 expression in normal and neoplastic tissues and its sensitivity and specificity in
603 prostate adenocarcinoma: an immunohistochemical study using multiple
604 tumour tissue microarray technique. *Histopathology* **2007**;50:472-83.
- 605 8. Minner S, Wittmer C, Graefen M, Salomon G, Steuber T, Haese A, *et al.* High
606 level PSMA expression is associated with early psa recurrence in surgically
607 treated prostate cancer. *Prostate* **2011**;71:281-8.
- 608 9. Ross JS, Sheehan CE, Fisher HA, Kaufman RP, Jr., Kaur P, Gray K, *et al.*
609 Correlation of primary tumor prostate-specific membrane antigen expression
610 with disease recurrence in prostate cancer. *Clin Cancer Res* **2003**;9:6357-62.
- 611 10. Liu H, Rajasekaran AK, Moy P, Xia Y, Kim S, Navarro V, *et al.* Constitutive
612 and antibody-induced internalization of prostate-specific membrane antigen.
613 *Cancer Res* **1998**;58:4055-60.
- 614 11. Rajasekaran SA, Anilkumar G, Oshima E, Bowie JU, Liu H, Heston W, *et al.* A
615 novel cytoplasmic tail MXXXL motif mediates the internalization of prostate-
616 specific membrane antigen. *Mol Biol Cell* **2003**;14:4835-45.
- 617 12. Smith-Jones PM, Vallabahajosula S, Goldsmith SJ, Navarro V, Hunter CJ,
618 Bastidas D, *et al.* In vitro characterization of radiolabeled monoclonal
619 antibodies specific for the extracellular domain of prostate-specific membrane
620 antigen. *Cancer Res* **2000**;60:5237-43.
- 621 13. Eder M, Schafer M, Bauder-Wust U, Hull WE, Wangler C, Mier W, *et al.* ⁶⁸Ga-
622 complex lipophilicity and the targeting property of a urea-based PSMA inhibitor
623 for PET imaging. *Bioconjug Chem* **2012**;23:688-97.
- 624 14. Zamboglou C, Drendel V, Jilg CA, Rischke HC, Beck TI, Schultze-Seemann
625 W, *et al.* Comparison of (⁶⁸Ga)-HBED-CC PSMA-PET/CT and multiparametric
626 MRI for gross tumour volume detection in patients with primary prostate
627 cancer based on slice by slice comparison with histopathology. *Theranostics*
628 **2017**;7:228-37.
- 629 15. Maurer T, Gschwend JE, Rauscher I, Souvatzoglou M, Haller B, Weirich G, *et*
630 *al.* Diagnostic Efficacy of (⁶⁸Gallium)-PSMA Positron Emission Tomography
631 Compared to Conventional Imaging for Lymph Node Staging of 130

- 632 Consecutive Patients with Intermediate to High Risk Prostate Cancer. *J Urol*
633 **2016**;195:1436-43.
- 634 16. Pyka T, Okamoto S, Dahlbender M, Tauber R, Retz M, Heck M, *et al.*
635 Comparison of bone scintigraphy and (68)Ga-PSMA PET for skeletal staging
636 in prostate cancer. *Eur J Nucl Med Mol Imaging* **2016**;43:2114-21.
- 637 17. Herlemann A, Wenter V, Kretschmer A, Thierfelder KM, Bartenstein P, Faber
638 C, *et al.* (68)Ga-PSMA Positron Emission Tomography/Computed
639 Tomography Provides Accurate Staging of Lymph Node Regions Prior to
640 Lymph Node Dissection in Patients with Prostate Cancer. *Eur Urol*
641 **2016**;70:553-7.
- 642 18. Perera M, Papa N, Roberts M, Williams M, Udovicich C, Vela I, *et al.* Gallium-
643 68 Prostate-specific Membrane Antigen Positron Emission Tomography in
644 Advanced Prostate Cancer-Updated Diagnostic Utility, Sensitivity, Specificity,
645 and Distribution of Prostate-specific Membrane Antigen-avid Lesions: A
646 Systematic Review and Meta-analysis. *Eur Urol* **2019**.
- 647 19. Hope TA, Aggarwal R, Chee B, Tao D, Greene KL, Cooperberg MR, *et al.*
648 Impact of (68)Ga-PSMA-11 PET on Management in Patients with
649 Biochemically Recurrent Prostate Cancer. *J Nucl Med* **2017**;58:1956-61.
- 650 20. Rahbar K, Ahmadzadehfar H, Kratochwil C, Haberkorn U, Schafer M, Essler
651 M, *et al.* German Multicenter Study Investigating 177Lu-PSMA-617
652 Radioligand Therapy in Advanced Prostate Cancer Patients. *J Nucl Med*
653 **2017**;58:85-90.
- 654 21. Baum RP, Kulkarni HR, Schuchardt C, Singh A, Wirtz M, Wiessalla S, *et al.*
655 177Lu-Labeled Prostate-Specific Membrane Antigen Radioligand Therapy of
656 Metastatic Castration-Resistant Prostate Cancer: Safety and Efficacy. *J Nucl*
657 *Med* **2016**;57:1006-13.
- 658 22. Baranski AC, Schafer M, Bauder-Wust U, Roscher M, Schmidt J, Stenau E, *et*
659 *al.* PSMA-11-Derived Dual-Labeled PSMA Inhibitors for Preoperative PET
660 Imaging and Precise Fluorescence-Guided Surgery of Prostate Cancer. *J Nucl*
661 *Med* **2018**;59:639-45.
- 662 23. Schottelius M, Wurzer A, Wissmiller K, Beck R, Koch M, Gorpas D, *et al.*
663 Synthesis and Preclinical Characterization of the PSMA-Targeted Hybrid
664 Tracer PSMA-I&F for Nuclear and Fluorescence Imaging of Prostate Cancer. *J*
665 *Nucl Med* **2019**;60:71-8.
- 666 24. Hell SW, Wichmann J. Breaking the diffraction resolution limit by stimulated
667 emission: stimulated-emission-depletion fluorescence microscopy. *Opt Lett*
668 **1994**;19:780-2.
- 669 25. Hell SW. Far-field optical nanoscopy. *Science* **2007**;316:1153-8.
- 670 26. Gorlitz F, Hoyer P, Falk HJ, Kastrup L, Engelhardt J, Hell SW. A STED
671 Microscope Designed for Routine Biomedical Applications. *Prog Electromagn*
672 *Res* **2014**;147:57-68.
- 673 27. Butkevich AN, Mitronova GY, Sidenstein SC, Klocke JL, Kamin D, Meineke
674 DN, *et al.* Fluorescent Rhodamines and Fluorogenic Carbopyronines for
675 Super-Resolution STED Microscopy in Living Cells. *Angew Chem Int Ed Engl*
676 **2016**;55:3290-4.
- 677 28. Hinner MJ, Johnsson K. How to obtain labeled proteins and what to do with
678 them. *Curr Opin Biotechnol* **2010**;21:766-76.
- 679 29. Benesova M, Schafer M, Bauder-Wust U, Afshar-Oromieh A, Kratochwil C,
680 Mier W, *et al.* Preclinical Evaluation of a Tailor-Made DOTA-Conjugated
681 PSMA Inhibitor with Optimized Linker Moiety for Imaging and
682 Endoradiotherapy of Prostate Cancer. *J Nucl Med* **2015**;56:914-20.

- 683 30. Baranski AC, Schafer M, Bauder-Wust U, Wacker A, Schmidt J, Liolios C, *et al.* Improving the Imaging Contrast of (68)Ga-PSMA-11 by Targeted Linker Design: Charged Spacer Moieties Enhance the Pharmacokinetic Properties. *Bioconjug Chem* **2017**;28:2485-92.
- 684
685
686
687 31. Gorges TM, Riethdorf S, von Ahsen O, Nastal YP, Rock K, Boede M, *et al.* Heterogeneous PSMA expression on circulating tumor cells: a potential basis for stratification and monitoring of PSMA-directed therapies in prostate cancer. *Oncotarget* **2016**;7:34930-41.
- 688
689
690
691 32. Dunn KW, Kamocka MM, McDonald JH. A practical guide to evaluating colocalization in biological microscopy. *Am J Physiol Cell Physiol* **2011**;300:C723-42.
- 692
693
694 33. Pastan IH, Willingham MC. Receptor-mediated endocytosis of hormones in cultured cells. *Annu Rev Physiol* **1981**;43:239-50.
- 695
696 34. Mellman I. Endocytosis and molecular sorting. *Annu Rev Cell Dev Biol* **1996**;12:575-625.
- 697
698 35. Bertelsen V, Sak MM, Breen K, Rodland MS, Johannessen LE, Traub LM, *et al.* A chimeric pre-ubiquitinated EGF receptor is constitutively endocytosed in a clathrin-dependent, but kinase-independent manner. *Traffic* **2011**;12:507-20.
- 699
700
701 36. Miller SE, Mathiasen S, Bright NA, Pierre F, Kelly BT, Kladt N, *et al.* CALM regulates clathrin-coated vesicle size and maturation by directly sensing and driving membrane curvature. *Developmental cell* **2015**;33:163-75.
- 702
703
704 37. Demandolx D, Davoust J. Multicolour analysis and local image correlation in confocal microscopy. *J Microsc-Oxford* **1997**;185:21-36.
- 705
706 38. Banerjee SR, Pullambhatla M, Byun Y, Nimmagadda S, Foss CA, Green G, *et al.* Sequential SPECT and optical imaging of experimental models of prostate cancer with a dual modality inhibitor of the prostate-specific membrane antigen. *Angewandte Chemie* **2011**;50:9167-70.
- 707
708
709
710 39. Gottfert F, Wurm CA, Mueller V, Berning S, Cordes VC, Honigmann A, *et al.* Coaligned dual-channel STED nanoscopy and molecular diffusion analysis at 20 nm resolution. *Biophys J* **2013**;105:L01-3.
- 711
712
713 40. Hotta J, Fron E, Dedecker P, Janssen KP, Li C, Mullen K, *et al.* Spectroscopic rationale for efficient stimulated-emission depletion microscopy fluorophores. *J Am Chem Soc* **2010**;132:5021-3.
- 714
715
716 41. Perico ME, Grasso S, Brunelli M, Martignoni G, Munari E, Moiso E, *et al.* Prostate-specific membrane antigen (PSMA) assembles a macromolecular complex regulating growth and survival of prostate cancer cells "in vitro" and correlating with progression "in vivo". *Oncotarget* **2016**;7:74189-202.
- 717
718
719
720 42. Schmidt S, Gericke B, Fracasso G, Ramarli D, Colombatti M, Naim HY. Discriminatory Role of Detergent-Resistant Membranes in the Dimerization and Endocytosis of Prostate-Specific Membrane Antigen. *PLoS One* **2013**;8:e66193.
- 721
722
723
724 43. Colombatti M, Grasso S, Porzia A, Fracasso G, Scupoli MT, Cingarlini S, *et al.* The prostate specific membrane antigen regulates the expression of IL-6 and CCL5 in prostate tumour cells by activating the MAPK pathways. *PLoS One* **2009**;4:e4608.
- 725
726
727

728

729 **Figure Legends**

730 **Fig. 1. Chemical structure and basic *in cellulo* characterization of STED-**
731 **compatible dual-labeled PSMA inhibitors. (A)** The conjugates consist of the PSMA
732 binding motif “Glu-urea-Lys” (orange), the radiometal chelator “HBED-CC” (gray) and
733 the fluorescence moiety “STAR RED” (red) or “STAR 635P” (blue) conjugated via
734 PEG₂ linker (black). **(B)** Confocal images of LNCaP and 22Rv1 cells after incubation
735 with 50 nM (LNCaP) and 250 nM (22Rv1) Glu-urea-Lys-HBED-CC-STAR RED for
736 15 min (LNCaP) and 45 min (22Rv1). Scale bars, 10 μm. **(C)** Frequency and **(D)**
737 duration of cell division of untreated (LNCaP, green: experiments *N*=13, divisions
738 *N*=347; 22Rv1, pale green: experiments *N*=6, divisions *N*=1029) and treated (100 nM
739 Glu-urea-Lys-HBED-CC-STAR RED, LNCaP, red: experiments *N*=16, divisions
740 *N*=624; 22Rv1, pale red: experiments *N*= 5, divisions *N*=1029 / 100 nM Glu-urea-Lys-
741 HBED-CC-STAR 635P, LNCaP, blue: experiments *N*=14, divisions *N*=408; 22Rv1,
742 pale blue: experiments *N*=5, divisions *N*=940) cells assessed by holographic time-
743 lapse cytometry. Box plot indicates the interquartile range (box), the outer-most data
744 points falling within 1.5× interquartile range (whiskers), the median (center line) and
745 the mean (triangle). Significance: * *p*<0.5, ** *p*<0.05, *** *p*<0.005. The results are
746 summarized in Table S3.

747

748 **Fig. 2. Organ distribution and small-animal PET imaging study of ⁶⁸Ga-labeled**
749 **STED-compatible dual-labeled PSMA inhibitors. (A)** Organ distribution and
750 corresponding tumor-to-organ (T/O) ratios of 60 pmol [⁶⁸Ga]Ga-Glu-urea-Lys-HBED-
751 CC-STAR RED (red) and [⁶⁸Ga]Ga-Glu-urea-Lys-HBED-CC-STAR 635P (blue) at 1 h
752 p.i.. Data are expressed as mean ± SD (*N*=3). The results are summarized in Table
753 S4. **(B)** From left to right: Confocal images of 5 nmol [⁶⁸Ga]Ga-Glu-urea-Lys-HBED-

754 CC-STAR RED (red) and DAPI (blue) in tumor tissue cryosections at 1 h p.i. and of
755 5 nmol [⁶⁸Ga]Ga-Glu-urea-Lys-HBED-CC-STAR RED (red) and autofluorescence
756 (green) in muscle tissue cryosections at 1 h p.i.. Scale bar, 10 μm. (C) Whole-body
757 maximum intensity projections of 0.5 nmol [⁶⁸Ga]Ga-Glu-urea-Lys-HBED-CC-
758 STAR RED (~50 MBq) in LNCaP- (left) and PC-3- (right) tumor-bearing athymic nude
759 mice (right trunk) 120 min p.i. obtained from small animal PET imaging. (D)
760 Corresponding time activity curves for tumor and muscle (left) and for other organs
761 (right). SUV=standardized uptake value.

762

763 **Fig. 3. STED imaging of Glu-urea-Lys-HBED-CC-STAR RED after PSMA binding**
764 **and clathrin-mediated endocytosis.** (A) Overview confocal (bottom) and STED
765 (top) image of LNCaP cells after incubation with 100 nM PSMA inhibitor for 45 min.
766 STED imaging resolves a heterogeneous distribution of PSMA inhibitor bound PSMA
767 with areas of higher and lower PSMA density. Marked membrane regions (dotted
768 cyan lines) in the overview are shown as magnified STED close-ups on the right.
769 Scale bar overview, 5 μm; scale bar close-ups, 2 μm. (B) Cytoplasmic vesicle shown
770 in confocal (top) and STED (bottom) mode exemplifying the resolution improvement
771 of STED. White arrows indicate the direction of line profiles (drawn on raw data)
772 depicted in (C) of the STED (orange) and confocal (gray) data. Pixel size is 20 nm for
773 both confocal and STED image. Scale bar, 250 nm. (D) Confocal image (left) of a
774 LNCaP cell after incubation with 100 nM PSMA inhibitor for 1 h at 37°C showing
775 different vesicle densities in the cytoplasm with accumulation favorably in filopodia.
776 The marked vesicles are depicted as STED close-ups on the right. Scale bar cell,
777 10 μm; scale bar vesicles, 250 nm. (E) To prove clathrin-mediated endocytosis,
778 colocalization between SNAP-tagged CLC labeled with 610CP (gray) and PSMA

779 inhibitor (red) was analyzed as illustrated in the sketch (top, ex – extracellular, cyto –
780 cytoplasm). Exemplary dual color live cell confocal image (bottom) of a CCV after
781 incubation with 50 nM PSMA inhibitor for 15 min. Scale bar, 500 nm. **(F)** Pearson's
782 correlation coefficient between SNAP-tagged CLC and PSMA inhibitor. Data are
783 expressed as mean \pm SD (10 min $N=7$, 15 min $N=14$). Significance: *** $p<0.005$. The
784 results are summarized in Table S6. **(G)** Size distribution of endoplasmic vesicles in
785 LNCaP (left) and 22Rv1 (right) cells after 30/45/60 min of internalization time with
786 100 nM PSMA inhibitor (ns – no significant differences). The fluorescence signal of
787 individual vesicles was fitted with a two-dimensional ring function (LNCaP: 30 min
788 $N=50$, 45 min $N=50$, 60 min $N=50$; 22Rv1: 30 min $N=81$, 45 min $N=38$, 60 min $N=59$).
789 Box plot indicates the interquartile range (box), the outer-most data points falling
790 within 1.5 \times interquartile range (whiskers), the median (center line) and the mean
791 (triangle). The results are summarized in Table S7. All STED data shown are
792 background corrected and linearly deconvolved. Fig. S7 illustrates the post
793 processing steps from raw data to background corrected and linearly deconvolved
794 data. All confocal data shown are raw data except for **(E)**.

795

796 **Fig. 4. Intracellular fate of the PSMA/PSMA inhibitor complex.** **(A)** Sketch of the
797 novel dual-staining approach targeting PSMA with indirect IF and PSMA inhibitor (ex
798 – extracellular, cyto – cytoplasm). **(B)** Definition of fluorogram sections (for details
799 see text). **(C)** Exemplary fluorograms (top) and corresponding STED images (bottom)
800 of LNCaP cells STAR 600-immunolabeled for PSMA (cyan) and co-incubated with
801 100 nM Glu-urea-Lys-HBED-CC-STAR RED (red) for different internalization times.
802 All scale bars, 5 μm . **(D)** Exemplary STED images of cytoplasmic vesicles in LNCaP
803 (top) and 22Rv1 (bottom) cells. After internalization, PSMA (cyan) and PSMA

804 inhibitor (red) first colocalize at the vesicle membrane (left). Within the first hour of
805 internalization, the PSMA/PSMA inhibitor complex segregates and the inhibitor
806 initially distributes homogeneously in the vesicles (right). Scale bar, 250 nm. **(E)**
807 Exemplary confocal images of LNCaP (top) and 22Rv1 (bottom) cells after 30 min
808 (left) and after 6 h of internalization of 100 nM Glu-urea-Lys-HBED-CC-STAR RED
809 (right) showing that the PSMA inhibitor eventually disperses in the cytoplasm. Scale
810 bar, 5 μ m. **(F)** Quantification of the extracellular (gray) and cytoplasmic ((pale)
811 orange) background of STED images of LNCaP cells (top) and of confocal images of
812 22Rv1 cells (bottom) after 30 min and after 6 h of incubation with 100 nM Glu-urea-
813 Lys-HBED-CC-STAR RED (LNCaP: ex 30 min $N=32$, cyto 30 min $N=32$, ex 6 h
814 $N=48$, cyto 6 h $N=48$; 22Rv1: ex 30 min $N=48$, cyto 30 min $N=48$, ex 6 h $N=88$, cyto
815 6 h $N=88$). Box plot indicates the interquartile range (box), the outer-most data points
816 falling within 1.5 \times interquartile range (whiskers), the median (center line) and the
817 mean (triangle). Significance: *** $p<0.005$. The results are summarized in Table S8.
818 All STED data shown are background corrected and linearly deconvolved. All
819 confocal data shown are raw data.

820

821 **Fig. 5. Endosomal recycling of PSMA after pH dependent PSMA/PSMA inhibitor**
822 **complex segregation.** **(A)** Exemplary confocal images (top) of living LNCaP (left)
823 and 22Rv1 (right) cells STAR 600-immunolabeled for PSMA (cyan) and incubated
824 with 500 nM LysoTrackerTM Green DND-26 (magenta) after >20 h internalization
825 time. Marked endosomes (white arrows) are depicted as close-ups (bottom) with
826 PSMA shown in STED mode and the STED-incompatible LysoTracker in confocal
827 mode. Exemplary LNCaP movie is supplied (Movie S5). Scale bar overview, 5 μ m;
828 scale bar close-ups, 500 nm. **(B)** Pearson's correlation coefficient between

829 immunolabeled PSMA and LysoTrackerTM Green DND-26 in living LNCaP and 22Rv1
830 cells. Data are expressed as mean \pm SD (LNCaP 1 h $N=21$, +20 h $N=26$; 22Rv1 1 h
831 $N=39$, +20 h $N=81$). Significance: *** $p<0.005$. The results are summarized in Table
832 S9. **(C)** Exemplary STED image of a LNCaP cell (left) and exemplary confocal image
833 of a 22Rv1 cell (right) STAR 600-immunolabeled for PSMA (cyan) and incubated with
834 100 nM Glu-urea-Lys-HBED-CC-STAR RED (red) for 1 h (LNCaP) and 6 h (22Rv1)
835 of internalization time. Marked regions (dotted yellow line) are depicted as STED
836 close-ups showing recycled PSMA at the cell membrane. Scale bar cell, 5 μm ; scale
837 bar close-ups, 2 μm . **(D)** Quantification of pH dependence of PSMA binding of the
838 primary and secondary antibody (either STAR RED- or STAR 600-labeled) complex,
839 Glu-urea-Lys-HBED-CC-STAR RED and -STAR 635P to LNCaP cells by flow
840 cytometry. Binding percentage was calculated based on normalizing binding to 100%
841 at pH 7.0. Data are expressed as mean \pm SD ($N=3$). Significance: ** $p<0.05$,
842 *** $p<0.005$. The results are summarized in Table S10. All STED data shown are
843 background corrected and linearly deconvolved. All confocal data shown are
844 background corrected. The LysoTrackerTM Green DND-26 confocal data of the
845 22Rv1 close-ups in **(A)** are additionally smoothed with a Gaussian low pass filter with
846 a width of one pixel.

Fig. 1

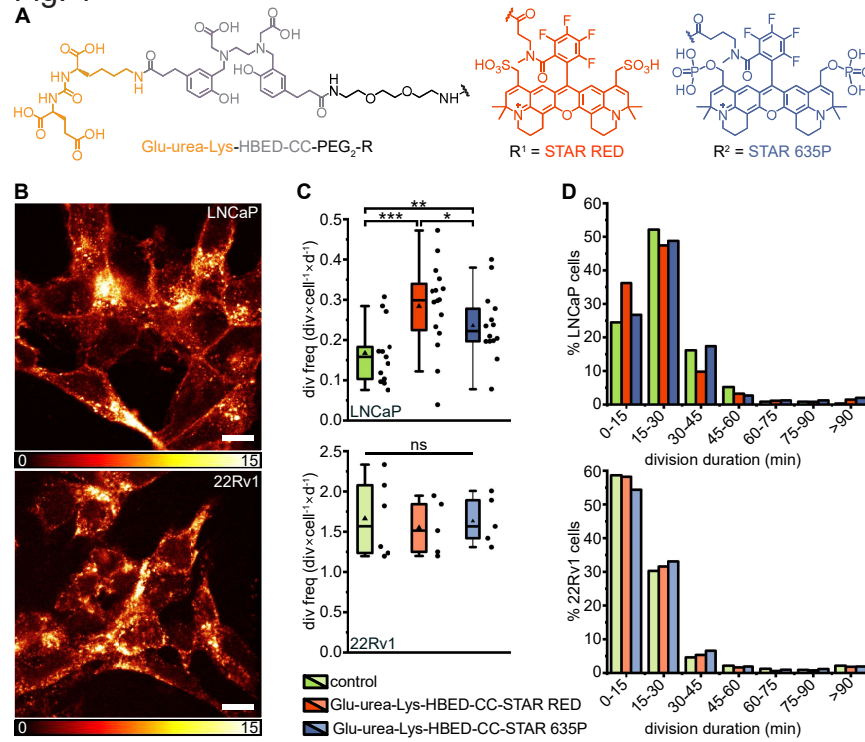


Fig. 2

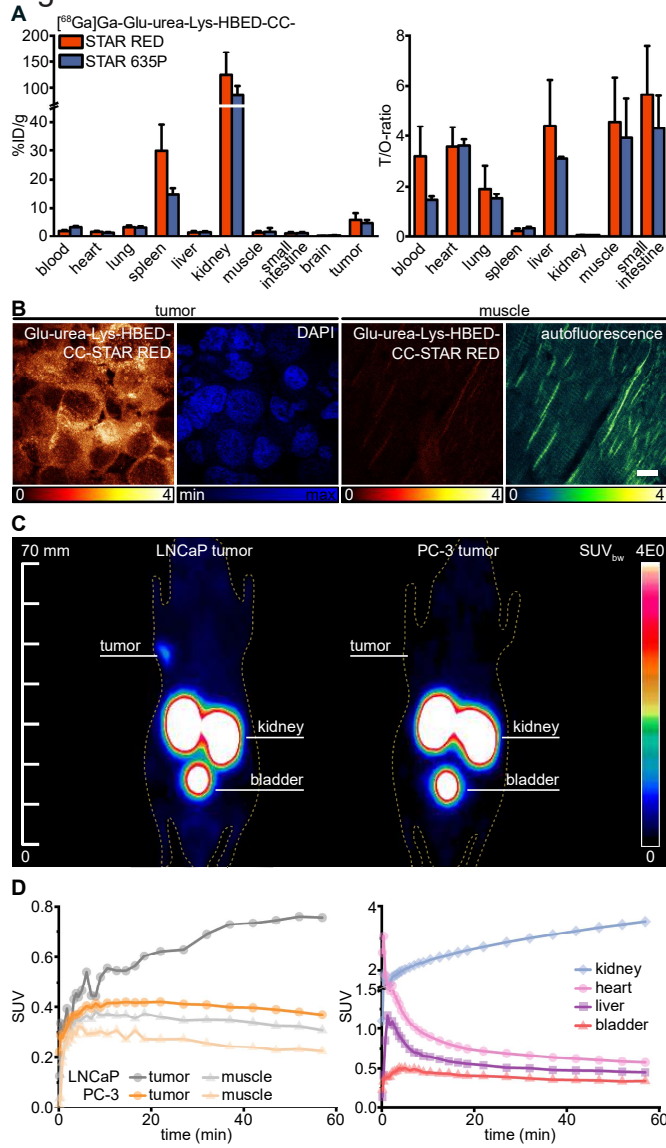


Fig. 3

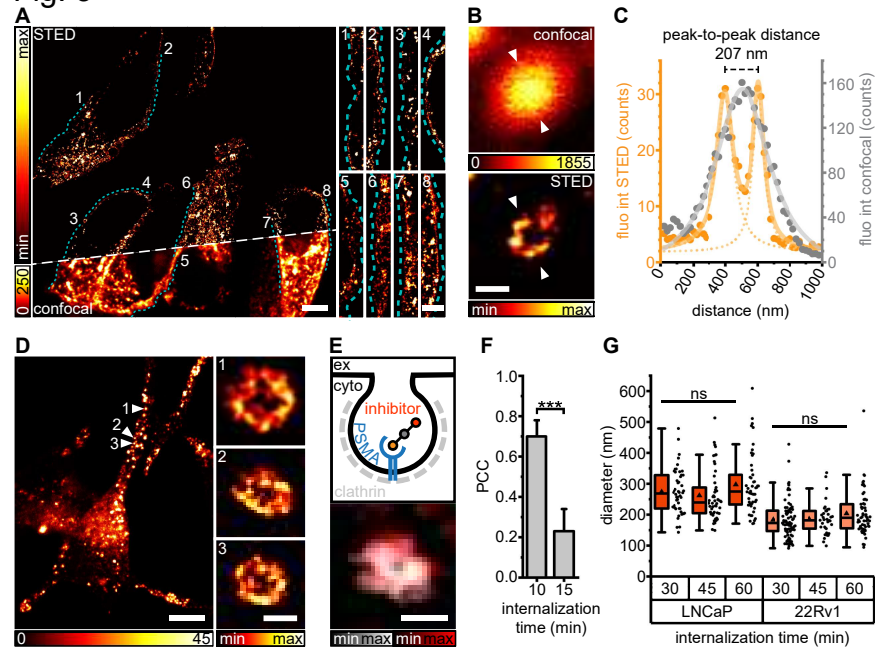


Fig. 4

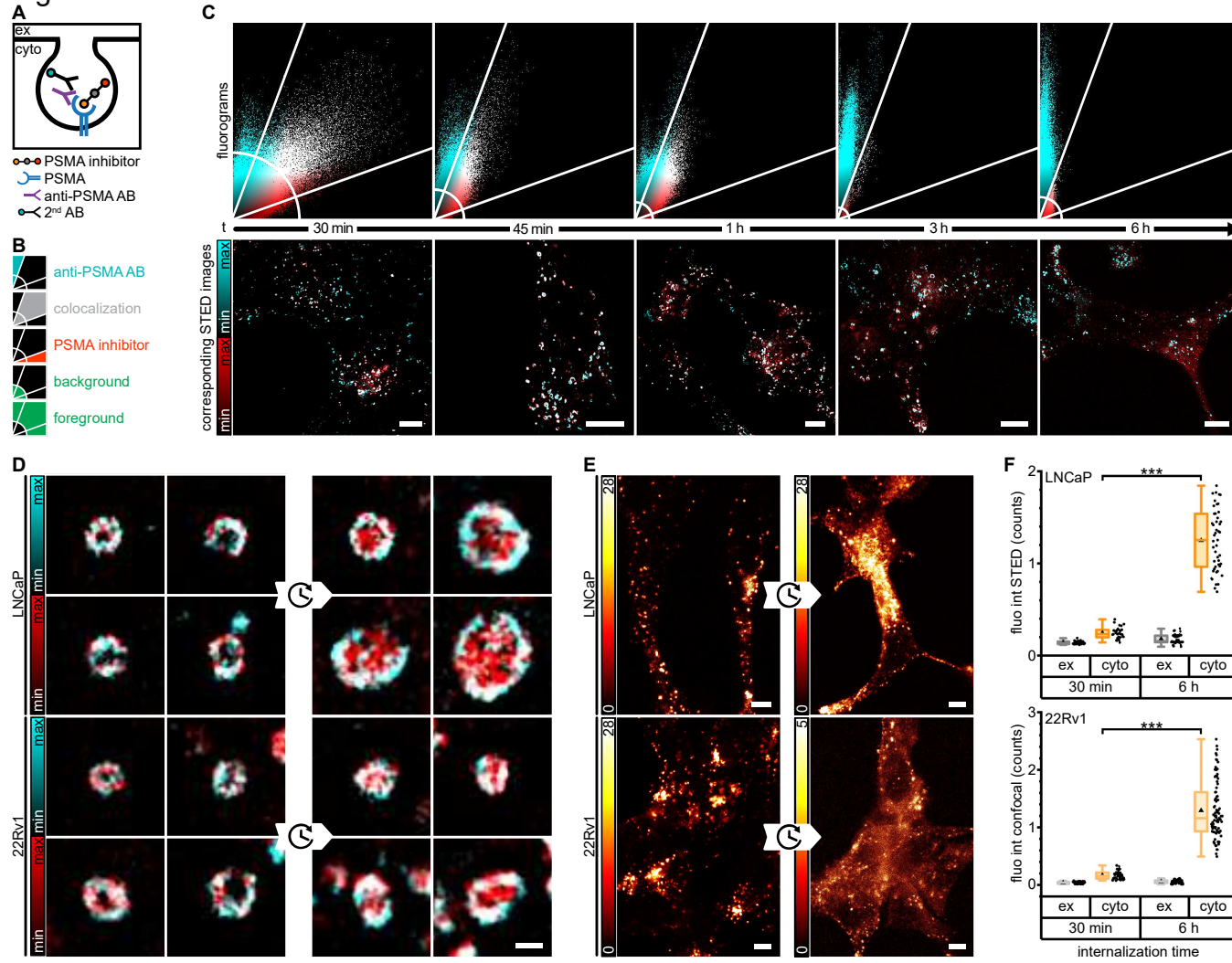


Fig. 5

